Electronic Materials Letters, Vol. 8, No. 6 (2012), pp. 587-593
DOI: 10.1007/s13391-012-2086-y

Reduction Synthesis of Tin Nanoparticles Using Various Precursors and Melting Behavior

Sang-Soo Chee and Jong-Hyun Lee*

Department of Materials Science & Engineering, Seoul National University of Science and Technology, Seoul 139-743, Korea

(received date: 16 May 2012 / accepted date: 12 June 2012 / published date: December 2012)

To achieve a more significant melting point drop through finer particles, chemical reduction synthesis of tin nanoparticles were conducted using four tin precursor agents: tin(II) acetate, tin(II) chloride, tin(II) sulfate, and tin(II) 2-ethylhexanoate. Depending on the precursor type, the sizes and size distributions of the synthesized Sn nanoparticles were highly diverse. Tin nanoparticles synthesized with tin(II) sulfate or tin(II) 2-ethylhexanoate displayed characteristics of monodispersity at reduced size. The nanoparticles had average diameters of just ~3 nm and ~6 nm, respectively, and exhibited melting points of 102.2°C and 131.1°C, which represented extreme drops by 130.4°C and 101.5°C in comparison with the melting point of bulk tin.

Keywords: solder, tin, nanoparticles, reduction synthesis, melting point

1. INTRODUCTION

Solder has been used as a key interconnection material in the electronics packaging field. Solder paste, which is deposited in patterns through a screen printing process, is a material directly related to attainment of fine pitch interconnection. Present solder pastes containing solder particles of a few tens of microns in size cannot meet ultrafine patterns of several tens of microns in pitch. Thus, preparing nanoscale solder particles is especially necessary to formulate solder pastes realizing the processability associated with ultrafine patterns.[1,2] Moreover, fabricating solder nanoparticles is directly linked to the production technology of conductive ink for jetting, which is a well-known non-contact metallization process.[3-5] It has been reported that inkjet technology promises the advantages of speed, simplicity, and low cost for fine pitch interconnection.

When the size of metal particles is under a few tens of nanometers, the melting point of the particles tends to decrease.[6-8] This is known as the melting drop phenomenon owing to miniaturization of particles, and it can be explained as the Gibbs-Thomson effect. Therefore, given solder nanoparticles with sizes under a few tens of nanometers, there might be a technique enabling not only fine pitch interconnection but also low temperature interconnection by using solder nanoparticles rather than an alloying method. The most frequently discussed preparation methods of Sn-based solder nanoparticles can be roughly classified into two approaches; namely, top-down and bottom-up.

Considering mass production and processing costs, the spark erosion method, which is a so-called arc discharge method, can be considered a good example of the top-down approach.[9-12] The method involves applying pulsed voltage between electrodes that are immersed in a dielectric medium (or solvent) and become sources of nanoparticles through induced metal transfer. This is similar in principle to gas metal arc welding (GMAW). If the current between the electrodes is sufficiently high, the spray mode of metal transfer is enabled and nanosized metal particles can form in the medium.

Andersson *et al.* reported that solder nanoparticles with composition Sn-0.4Co-0.7Cu were formed using a spark erosion method.[9] However, the minimum melting point was measured as 224°C, which is only 5.3°C lower than that of the bulk material, because the size variation of the synthesized nanoparticles was very great and the minimum size of the particles exceeded 20 nm. Thus, no pronounced melting point drop was observed. Zou *et al.* performed tests of Sn-3.0Ag-0.5Cu, which is the most conventionally used Pb-free solder composition, with a melting point of 217°C.[12] The average diameter of the nanoparticles was observed as 30 nm, which corresponded to a slight melting point drop by 3°C.[12] These results indicated the limitations of the spark erosion process with regard to uniformity and minuteness in

*Corresponding author: pljh@seoultech.ac.kr
©KIM and Springer

the sizes of the synthesized particles.

The best known example of the bottom-up approach is a reduction synthesis method using a chemical wet process, including a polyol method.[13-21] This process comprises decomposition of the precursor and reduction of metal ions in the solvent. In the process, a surfactant (or capping agent) is usually added during the reduction synthesis to promote nucleation by metal ions, suppress agglomeration between nanoparticles, and prevent excessive oxidation with formed nanoparticles.

Jiang *et al.* synthesized Sn nanoparticles via chemical reduction using anhydrous methanol, and with the optimum molar ratio between the surfactant and the tin(II) acetate precursor an average diameter of 26 nm was observed.[13] Hence, the melting point of pure Sn nanoparticles was measured as 214.9°C, which is 17.7°C lower than that of bulk Sn. Subsequently, Huang *et al.* tried a synthesis method that involved mixing tin chloride precursor with excess reductant in a reaction bath, and they reported the formation of the uniform-sized finest Sn nanoparticles with an average diameter of 10.4 nm.[16] However, the melting point was not reported. Recently, through a modified polyol method in which reductant solution was injected, Jo *et al.* synthesized fine Sn-Cu nanoparticles with typical diameters from 13.4 to 14.2 nm.[21] The minimum melting point was measured as 200.3°C, thus a significant melting point drop of ~30.3°C was achieved. These results implied that reduction synthesis is one of the most viable fabrication methods since mass production and large melting point drop are possible simultaneously.

However, the Sn precursors available for the chemical reduction are very diverse. Actually, different Sn precursors have already been used in the process.[13-21] Hence, there is a need to elucidate the effects of each precursor type on the synthesis. In this study, trends in synthesized Sn nanoparticles were observed with respect to Sn precursor type. Moreover, the melting point drop of the synthesized Sn nanoparticles was measured for each Sn precursor type and then analyzed on that basis.

2. EXPERIMENTAL PROCEDURE

In this study, four agents were used as precursors: tin(II) acetate ($Sn[CH_3CO_2]_2$) (not reported for putity), tin(II) chloride ($SnCl_2$) (98%), tin(II) sulfate ($SnSO_4$) (>95%), and tin(II) 2-ethylhexanoate ($[CH_3(CH_2)_3CH(C_2H_5)CO_2]_2Sn$) (~95%). All precursors were purchased from Sigma-Aldrich Co. and used as received without further processing or purification. In addition, diethylene glycol (DEG) (99%, Sigma-Aldrich Co.), polyvinylpyrrolidone (PVP) (molecular weight 1300000, Aldrich Chemical Co.), and sodium borohydride ($NaBH_4$) (99.99%, Sigma-Aldrich Co.) were used as a solvent, capping material, and reducing agent, respectively.

Sn nanoparticles were synthesized via chemical reduction at room temperature by injection of DEG solution containing tin salts into DEG solution containing PVP and sodium borohydride. To prepare the DEG containing PVP and sodium borohydride, 0.015 g of PVP and 0.5 g of sodium borohydride were completely dissolved in 2 mL of DEG. Each Sn precursor was dissolved in 8 ml of DEG. Because tin(II) 2-ethylhexanoate is a liquid, this was directly injected into 10 mL of DEG containing PVP and sodium borohydride without further processing. Table 1 summarizes the synthesis conditions according to precursor type. The concentration of all precursors on the final solution (~10 mL) basis was equal to 0.25 mol. The injection of precursor solution using a dispenser was performed at the rate of ~0.45 mL/s. However, due to its high viscosity, tin(II) 2-ethylhexanoate was injected at ~0.06 mL/s. In order to complete the reaction, the DEG solution was continuously stirred using a magnetic bar from the moment of injection until 90 min later.

After the synthesis, the DEG solutions containing Sn nanoparticles were dripped on copper grids coated with carbon film to prepare samples for analysis with a high-resolution transmission electron microscope (HR-TEM) (Tecnai 20, FEI Co.) operated at 200 kV.

For analysis with a differential scanning calorimeter (DSC) (Q20, TA Instruments) to measure the melting points of the nanoparticles, the DEG solutions containing synthesized Sn nanoparticles underwent a relatively low centrifuge speed of 6000 rpm for 30 min to minimize agglomeration between nanoparticles. To allow free evaporation of DEG, no lid was used on the sample pan during the measurement. The initial sample mass was 10 mg and heating from 30°C to 250°C was at the rate of 10°C/min. To prevent oxidation during the heating, nitrogen gas was blown with a rate of

Table 1. Case summary of reduction synthesis conducted in this study.

Precursor (g)		DEG (mL)		PVP (g)	$NaBH_4$ (g)
		For precursor solution	For PVP/$NaBH_4$ solution		
Tin(II) acetate	0.5920	8	2	0.015	0.5
Tin(II) chloride	0.4741	8	2		
Tin(II) sulfate	0.5369	8	2		
Tin(II) 2-ethylhexanoate	-	0.81	10		

50 mL/min. This method of measurement can provide the best results for melting point drop, because agglomeration between particles during an implicit drying step is avoided. Moreover, the results of the measurement can be directly connected with the sintering temperature of Sn ink.

3. RESULTS AND DISCUSSION

Figure 1 shows TEM images of Sn nanoparticles synthesized using the four types of Sn precursor. In the case of the tin(II) acetate precursor (Fig. 1(a)), the sizes of the nanoparticles varied from a few nanometers to 45 nm, and thus, the divergence in size was appreciable. The sizes of the particles synthesized with tin(II) chloride (Fig. 1(b)) were observed to range from 2 nm to 60 nm, also representing a wide distribution in size. Even so, most of the particles analyzed were between 10 nm and 18 nm in size. Conversely, the sample prepared with tin(II) sulfate (Fig. 1(c)) represented a formation of very fine nanoparticles with diameters of several nanometers in general, although some nanoparticles had started to agglomerate partially. Finally, the nanoparticles synthesized using tin(II) 2-ethylhexanoate (Fig. 1(d)) were highly discrete and most of these round nanoparticles were measured as <10 nm in size.

The TEM results examined indicate that the sizes and size distributions of Sn nanoparticles synthesized via chemical reduction differ remarkably with respect to the precursor type. The extremely polydisperse nanoparticles obtained using tin(II) acetate and tin(II) chloride precursors can be interpreted as the results of multiple nucleation events during extended nucleation periods. The reduction process of Sn ions supplied from the precursor could be represented by the reaction:[14]

$$BH_4^- + 8OH^- + 4Sn^{2+} \rightarrow B(OH)_4^- + 4H_2O\ (g) + 4Sn. \quad (1)$$

Reaction (1) is divided into next two reactions:

$$BH_4^- + 8OH^- \rightarrow B(OH)_4^- + 4H_2O + 8e^- \quad (2)$$

$$4Sn^{2+} + 8e^- \rightarrow 4Sn. \quad (3)$$

Reaction (2) occurs at the DEG solution with sodium borohydride. Another solution containing Sn salts was injected into the mixture solution of PVP and sodium borohydride. Then, the Sn ions were consumed for nucleation and growth processes after reaction (3). The metal ions would be simultaneously reduced to metal species in the presence of sufficient reducing agent, followed immediately by conversion to stable nuclei by growth of the metal species. Generally, this proceeds over a short period of time. Then, the stable nuclei would also continuously grow into nanosized particles with the addition of the Sn species until the concentration of the metal species fell to a saturation level.

Hence, the size distribution of the synthesized Sn nanoparticles can be explained using a LaMer model of the nucleation and growth stages, as shown in Fig. 2.[22,23] When the reduction rate of Sn ions surpasses the consumption rate of Sn species due to growth, the concentration of reduced Sn species remains above the critical supersaturation concentration (or nucleation concentration) for a certain time, and then the concentration fluctuates about the critical supersaturation level. This implies that an extended nucleation or multiple nucleation events also occur during the growth into nano-

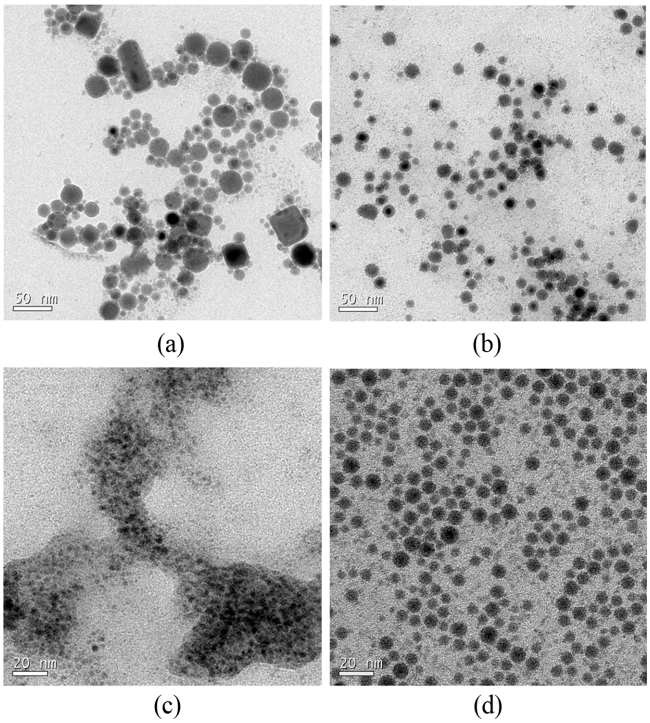

Fig. 1. TEM images of Sn nanoparticles synthesized using four types of tin precursor: (a) tin(II) acetate, (b) tin(II) chloride, (c) tin(II) sulfate, and (d) tin(II) 2-ethylhexanoate.

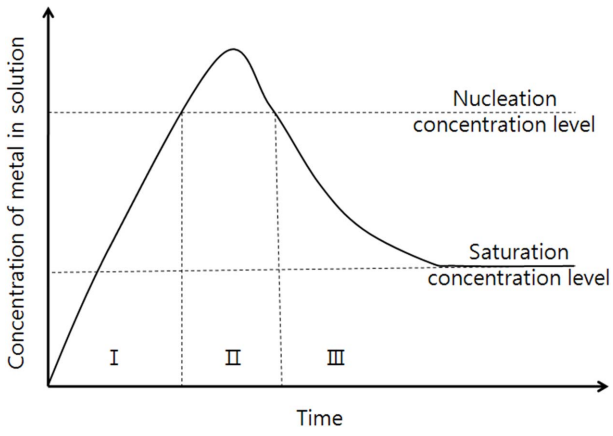

Fig. 2. LaMer diagram to explain variation in particle size distribution through homogeneous nucleation and growth: I) pre-nucleation stage; II) nucleation stage; and III) growth stage.[21,22]

sized particles. In other words, nucleation and growth are not completely separate stages in this case. The particles formed beforehand continue to grow gradually over time until the ionic species or reducing agent is exhausted. Consequently, the different growing period of each nucleus would result in a broader size distribution among the synthesized Sn particles.[24] In this study, use of tin(II) acetate and tin(II) chloride precursors is judged to have fallen into this case.

If the reduction rate of Sn ions is lower than the consumption rate of Sn species due to growth, the concentration of reduced Sn species drops rapidly below the nucleation concentration and finally to the saturation concentration after a short burst of nucleation. In this case, only continuous growth behavior without additional nucleation would be exhibited after a very short nucleation stage, resulting in a narrow size distribution. In our experiments, the synthesis using tin(II) sulfate or tin(II) 2-ethylhexanoate precursors is believed relevant to this case. The finer size of the Sn nanoparticles synthesized using tin(II) sulfate and tin(II) 2-ethylhexanoate is likely attributable to the relatively high nucleation rate and resultant increase in the number of nuclei, which accelerated the lowering of the concentration of Sn species to the saturation level, permitting a short growth period. It is believed that the difference in reduction rates of Sn ions with different precursors is mainly attributed to the purity of precursor materials. Impurity ions prepared from relatively low-purity precursors (tin(II) sulfate and tin(II) 2-ethylhexanoate) may disrupt the reduction reaction represented by eqaution (3) and reduce the reduction rate.[25]

In previous experiments using tin(II) acetate, Sn nanoparticles synthesized in anhydrous methanol exhibited a wide size distribution similar to our result,[13] while Sn-0.7Cu nanoparticles synthesized in 1,5 pentanediol represented monodisperse nanoparticles of 14 nm to 21 nm.[21] Therefore, it is also judged that the characteristic size and size distribution of the nanoparticles are also dependent strongly on the solvent type in the reduction synthesis.

To attempt thermal analysis of each solution containing Sn nanoparticles, a DSC measurement of the solvent itself was conducted. Figure 3 shows a DSC result measured for DEG, which is the solvent used in this study. The DEG presented a wide endothermic peak from ~80°C to 183.5°C owing to its evaporative behavior. During further heating, this endothermic peak abruptly disappeared because of complete evaporation of the DEG.

DSC results for DEG solutions containing Sn nanoparticles synthesized using the Sn precursors are shown in Figs. 4 to 7. For the solution containing nanoparticles synthesized with tin(II) acetate precursor, notable endothermic peaks were observed at 97.2°C and 204.1°C during the first scan of the DSC measurement, as observed in Fig. 4, when the endothermic peak due to evaporation of DEG was expected.

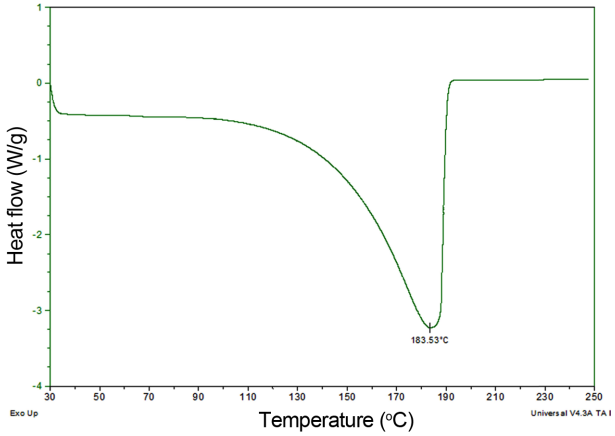

Fig. 3. DSC result for DEG.

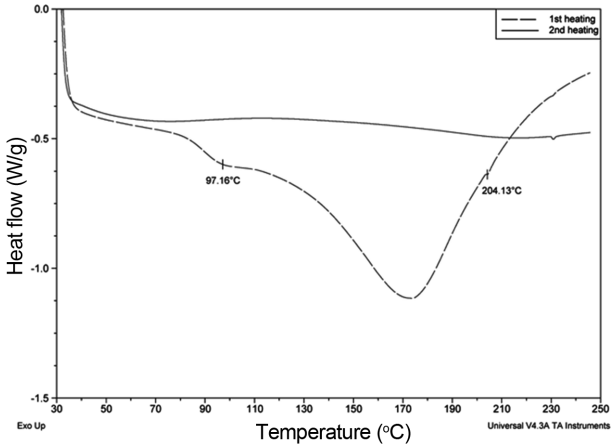

Fig. 4. DSC result for DEG solution containing Sn nanoparticles synthesized from tin(II) acetate.

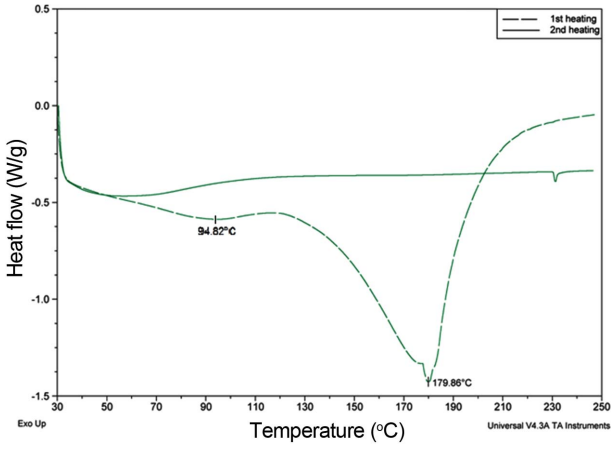

Fig. 5. DSC result for DEG solution containing Sn nanoparticles synthesized from tin(II) chloride.

From estimation by the Hanszen model and experimental results, Lai *et al.* reported that pure Sn nanoparticle of

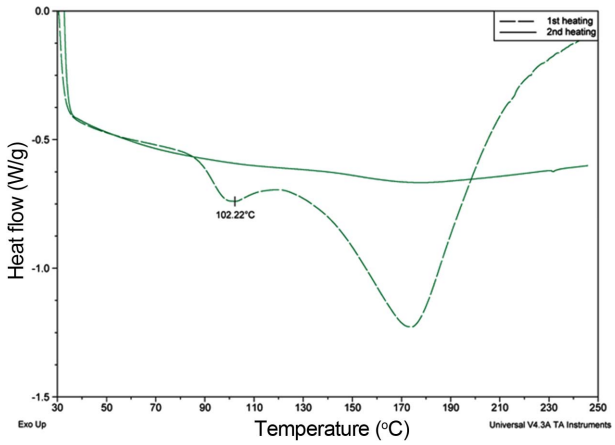

Fig. 6. DSC result for DEG solution containing Sn nanoparticles synthesized from tin(II) sulfate.

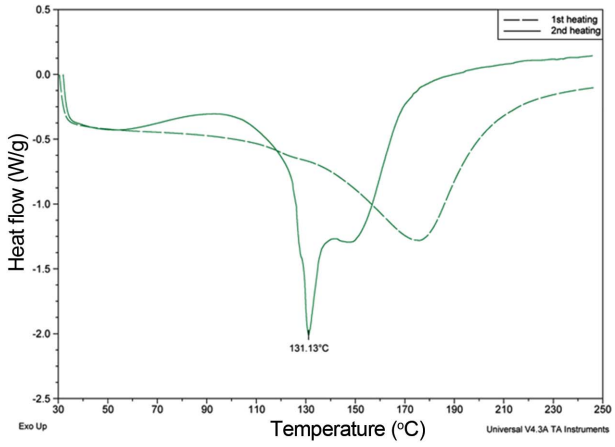

(a)

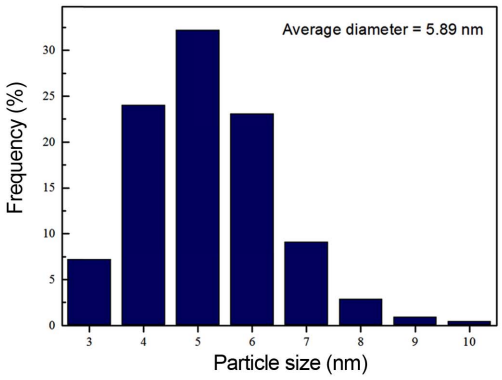

(b)

Fig. 7. (a) DSC result for DEG solution containing Sn nanoparticles synthesized from tin(II) 2-ethylhexanoate and (b) size distribution of the Sn nanoparticles.

~50 nm in diameter had an insignificant melting point drop, while Sn nanoparticle of ~10 nm had a significant melting point drop.[24] Hence, the peak detected at 97.2°C was found to correspond with the nanoparticles of a few nanometers shown in Fig. 1(a). Moreover, the peak at 204.1°C was considered an effect due to some nanoparticles of ~17 nm. While two peaks related to nanoparticles were observed during the first heating, no additional peaks were observed during the second heating, except for an endothermic peak due to normal melting of Sn at 232.6°C. The Sn nanoparticles melted during the first heating immediately agglomerated with each other and transformed into larger particles.[3] As a result, the agglomerated nanoparticles eventually lost the melting point drop and resumed the melting characteristics of bulk Sn during the second heating.

For the sample fabricated from tin(II) chloride (Fig. 5), a dim and sharp endothermic peak superposed on the evaporation peak of DEG was detected at 94.8°C and 179.9°C, respectively, during the first heating. In view of Fig. 1(b), this peak was estimated to correspond with nanoparticles of a few nanometers and ~13 nm in diameter, respectively. For the reason mentioned above, the melting drop characteristics of the nanoparticles vanished during the second heating, with then melting at 232.6°C.

In the DSC result for nanoparticles synthesized using tin(II) sulfate precursor, a distinct endothermic peak was detected at 102.2°C, as shown in Fig. 6, implying the formation of very fine Sn nanoparticles. This supposition is well confirmed by the image shown in Fig. 1(c). Therefore, a drastic melting point drop of 130.4°C was realized, which is a result that has never been reported before. During the second heating, no other peaks were observed, except for the normal melting peak of Sn.

Finally, the sample prepared with tin(II) 2-ethylhexanoate revealed no distinct peaks except for the evaporation peak of DEG and a slight feature at ~130°C during the first heating (Fig. 7a). However, a sharp endothermic peak was detected at 131.1°C during the second heating performed after the elimination of DEG, and this indicated a remarkable melting point drop of 101.5°C by the remaining Sn nanoparticles. The extremely slight melting peak observed during the first heating is probably due to the relatively lower amount of Sn nanoparticles. The average size of the Sn nanoparticles in Fig. 1(d) was measured as ~6 nm, as shown in Fig. 7(b), which is consistent with the observed melting point drop. For this sample, the cause of the retarded agglomeration among nanoparticles is mainly attributed to the highly isolated arrangement of each nanoparticle. The placement of Sn nanoparticles observed in Fig. 1(d) represents great isolation and discreteness with no aggregation, whereas most of the nanoparticles observed in the other samples represented partially aggregated or linked forms. Hence, it was anticipated that the sample in Fig. 1(d) would offer greater resistance against the agglomeration by heating for a longer time or at higher temperature. Consequently, unlike the other samples, that in Fig. 1(d) suffered no pronounced agglomeration dur-

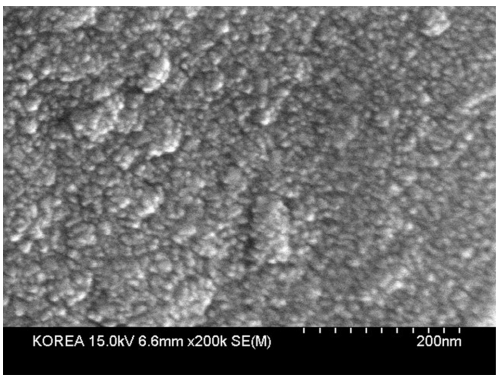

Fig. 8. SEM micrograph showing appearance of Sn nanoparticles stnthesized from tin(II) 2-ethylhexanoate after the first heating.

ing the evaporation of DEG by the first heating.

Figure 8 shows a field-emission SEM image of Sn nanoparticles prepared with tin(II) 2-ethylhexanoate after first heating. Although the sticky surface characteristics of Sn nanoparticles encapsulated with PVP enhanced the aggregation among the surfaces of nanoparticles during drying due to the heating, the SEM image demonstrated that the size of Sn nanoparticles was maintained even after the heating, corresponding to the endothermic peak at 131.1°C measured during the second heating.

The above-mentioned results are summarized in Table 2. Even though the size distributions were different, very fine particles of several nanometers were observed in all samples. Moreover, based upon the endothermic peaks detected at the lowest temperatures, the samples showed drastic melting point drops. In particular, the Sn nanoparticles synthesized with tin(II) sulfate or tin(II) 2-ethylhexanoate exhibited the characteristic of fine size with a relatively narrow size distribution. Sn nanoparticles synthesized using tin(II) sulfate and tin(II) 2-ethylhexanoate had small average diameters of ~3 nm and ~6 nm, respectively; this indicates a melting points of 102.2°C and 131.1°C, which is lower by 130.4°C and 101.5°C than that of bulk Sn. It was also confirmed that the most frequently detected size of the synthesized nanoparticles was compatible with the melting point expected from the previous results of simulations and experiments by other researchers.[11,12,26]

4. CONCLUSIONS

Results were obtained from the analysis of Sn nanoparticles synthesized via chemical reduction using four tin precursor agents: tin(II) acetate, tin(II) chloride, tin(II) sulfate, and tin(II) 2-ethylhexanoate. Depending on the precursor type, the sizes and size distributions of the synthesized Sn nanoparticles were highly diverse. In the case of tin(II) acetate or tin(II) chloride, the synthesized Sn nanoparticles exhibited polydisperse characteristics, with an extremely wide range in size. By contrast, Sn nanoparticles synthesized using tin(II) sulfate or tin(II) 2-ethylhexanoate exhibited monodisperse characteristics, with an exceedingly fine size. For example, Sn nanoparticles synthesized using tin(II) sulfate and tin(II) 2-ethylhexanoate had average diameters of ~3 nm and ~6 nm, respectively, and melting points of 102.2°C and 131.1°C, which represented considerable drops by 130.4°C and 101.5°C in comparison with the melting point of bulk Sn.

ACKNOWLEDGMENTS

This study was supported by the National Research Foundation of Korea funded by the Ministry of Education, Science and Technology (2011-0009088).

REFERENCES

1. E. H. Amalu, W. K. Lau, N. N. Ekere, R. S. Bhatti, S. Mallik, K. C. Otiaba, and G. Takyi, *Microelectron. Eng.* **88**, 1610 (2011).
2. T N. Tsai, *Robot. Comput. Integrated Manuf.* **27**, 808 (2011).
3. Y. H. Jo, I. Jung, C. S. Choi, I. Kim, and H. M. Lee, *Nanotechnology* **11**, 1037 (2011).
4. M. S. Cho, W. H. Choi, S. G. Kim, I. H. Kim, and Y. Lee, *J. Nanosci. Nanotechno.* **10**, 6888 (2010).
5. A. Gupta, A. S. G. Khalil, M. Offer, M. Geller, M. Winterer, A. Lorke, and H. Wiggers, *J. Nanosci. Nanotechno.* **11**, 5028 (2011).
6. M. Takagi, *J. Phys. Soc. Jpn.* **9**, 2011 (1954).
7. K. J. Hanszen, *Z. Phys.* **157**, 523 (1960).
8. P. Buffat and J. P. Borel, *Phys. Rev. A* **13**, 2287 (1976).

Table 2. Size distributions and minimum melting points of synthesized Sn nanoparticles as functions of precursor type.

	Size distribution by diameter (nm)	Most frequently detected size by diameter (nm)	Measured minimum melting point (°C)
Tin(II) acetate	2-45	<3 or ~17	97.2
Tin(II) chloride	2-60	<3 or ~13	94.8
Tin(II) sulfate	2-4	~3	102.2
Tin(II) 2-ethylhexanoate	3-10	~5	131.1

9. C. Andersson, C. Zou, B. Yang, Y. Gao, J. Liu, and Q. Zhai, *Proc. 2nd ESTC*, p. 915, IEEE, Greenwich, UK (2008).
10. C. D. Zou, Y. L. Gao, B. Yang, Q. J. Zhai, C. Andersson, and J. Liu, *Solder. Surf. Mount Technol.* **21**, 9 (2009).
11. Y. Gao, C. Zou, B. Yang, Q. Zhai, J. Liu, E. Zhuravlev, and C. Schick, *J. Alloys Compd.* **484**, 777 (2009).
12. C. D. Zou, Y. L. Gao, B. Yang, X. Z. Xia, Q. J. Zhai, C. Andersson, and J. Liu, *J. Electron. Mater.* **38**, 351 (2009).
13. H. Jiang, K. Moon, H. Dong, F. Hua, and C. P. Wong, *Chem. Phys. Lett.* **429**, 492 (2006).
14. L. Y. Hsiao and J. G. Duh, *J. Electron. Mater.* **35**, 1755 (2006).
15. H. Jiang, K. Moon, F. Hua, and C. P. Wong, *Chem. Mater.* **19**, 4482 (2007).
16. P. C. Huang and J. G. Duh, *Proc. 58th ECTC*, p. 431, IEEE CPMT, Orlando, US (2008).
17. H. Jiang, K. Moon, and C. P. Wong, *Proc. 58th ECTC*, p. 1400, IEEE CPMT, Orlando, US (2008).
18. C. Y. Lin, U. S. Mohanty, and J. H. Chou, *J. Alloys Compd.* **472**, 281 (2009).
19. C. Zou, Y. Gao, B. Yang, and Q. Zhai, *J. Mater. Sci.: Mater. Electron.* **21**, 868 (2010).
20. C. Y. Lin, U. S. Mohanty, and J. H. Chou, *J. Alloys Compd.* **501**, 204 (2010).
21. Y. H. Jo, J. C. Park, J. U. Band, H. Song, and H. M. Lee, *J. Nanosci. Nanotechno.* **11**, 1037 (2011).
22. V. K. LaMer and R. H. Dinegar, *J. Am. Chem. Soc.* **72**, 4847 (1950).
23. V. K. LaMer, *Ind. Eng. Chem.* **44**, 1270 (1952).
24. B. K. Park, S. Jeong, D. Kim, J. Moon, S. Lim, and J. S. Kim, *J. Colloid Interface Sci.* **311**, 417 (2007).
25. J. J. Zhu, H. Wang, S. Xu, and H. Y. Chen, *Langmuir* **18**, 3306 (2002).
26. S. L. Lai, J. Y. Guo, V. Petrova, G. Ramanath, and L. H. Allen, *Phys. Rev. Lett.* **77**, 99 (1996).